

Lattice Distortion and Resonant X-Ray Scattering in DyB₂C₂

Jun-ichi IGARASHI* and Tatsuya NAGAO¹

Synchrotron Radiation Research Center, Japan Atomic Energy Research Institute, Mikazuki, Sayo, Hyogo 679-5148

¹*Faculty of Engineering, Gunma University, Kiryu, Gunma 376-8515*

(Received January 6, 2003)

We study the resonant x-ray scattering (RXS) spectra at the Dy L_{III} absorption edge in the quadrupole ordering phase of DyB₂C₂. Analyzing the buckling of sheets of B and C atoms, we construct an effective model that the crystal field is acting on the $5d$ and $4f$ states with the principal axes different for different sublattices. Treating the $5d$ states as a band and the $4f$ states as localized states, we calculate the spectra within the dipole transition. We take account of processes that (1) the lattice distortion directly modulates the $5d$ states and (2) the charge anisotropy of the quadrupole ordering $4f$ states modulates the $5d$ states through the $5d$ - $4f$ Coulomb interaction. Both processes give rise to the RXS intensities on $(00\frac{\ell}{2})$ and $(h0\frac{\ell}{2})$ spots. Both give similar photon-energy dependences and the same azimuthal-angle dependences for the main peak, in agreement with the experiment. The first process is found to give the intensities much larger than the second one in a wide parameter range of crystal field. This suggests that the main-peak of the RXS spectra is not a direct reflection of the quadrupole order but mainly controlled by the lattice distortion.

KEYWORDS: resonant X-ray scattering, DyB₂C₂, lattice distortion, Dy L_{III} absorption edge

1. Introduction

Resonant x-ray scattering has recently attracted much interest, since the resonant enhancement for the prohibited Bragg reflection corresponding to the orbital order has been observed in several transition-metal compounds by using synchrotron radiation with photon energy around the K absorption edge.¹⁻⁴ For such K -edge resonances, $4p$ states of transition metals are involved in the intermediate state in the electric dipolar (E_1) process, and they have to be modulated in accordance with the orbital order for the signal to be observed. This modulation was first considered to come from the anisotropic term of the $4p$ - $3d$ intra-atomic Coulomb interaction,⁵ but subsequent studies based on the band structure calculation⁶⁻⁹ have revealed that the modulation comes mainly from the crystal distortion via the oxygen potential on the neighboring sites. This is because $4p$ states are so extending in space that they are very sensitive to the electronic structure at neighboring sites.

Rare-earth compounds also show the orbital order (usually an ordering of quadrupole moments). In CeB₆, RXS experiments were carried out around the Ce L_{III} absorption edge, and resonant enhancements have been found on quadrupolar ordering superlattice spots.¹⁰ Only one peak appeared as a function of photon energy, which was assigned to the E_1 process. In the E_1 process, $5d$ states of Ce in the intermediate state are to be modulated in accordance with the superlattice spots. Since the lattice distortion seems extremely small and the $5d$ states are less extending than the $4p$ states in transition-metal compounds, it is highly possible that the modulation is mainly caused by the Coulomb interaction between the $5d$ states and the orbital ordering $4f$ states. In our previous papers,^{11,12} we demonstrated this scenario by calculating the RXS spectra on the basis of the effective Hamiltonian of Shiina et al.¹³⁻¹⁵ Without the

help of lattice distortion, we obtained sufficient intensities of the spectra, and reproduced well the temperature and magnetic field dependences. This situation contrasts with those in transition-metal compounds.

Another example for rare-earth compounds is RXS experiments on DyB₂C₂, where the intensity is resonantly enhanced near the Dy L_{III} absorption edge.¹⁶⁻¹⁸ This material takes a tetragonal form at high temperatures as shown in Fig. 1(a), and undergoes two phase transitions with decreasing temperatures in the absence of the magnetic field: a quadrupole order below T_Q ($= 24.7$ K) (Phase II) and a magnetic order below T_C ($= 15.3$ K) (Phase III).¹⁹ Corresponding to the transition at T_Q , a large non-resonant intensity is found in the $\sigma \rightarrow \sigma'$ channel on the $(h0\frac{\ell}{2})$ spot (h and ℓ are odd integers).¹⁸ This suggests that some structural change takes place at $T = T_Q$ from the tetragonal phase at high temperatures.^{16,17} A buckling of sheets of B and C atoms was proposed,¹⁶ and the non-resonant intensities by the buckling has recently been evaluated; about 0.01 Å shift of B and/or C atoms may be sufficient to give rise to such large intensities.²⁰ It is not clear in experiments whether the intensity on this spot is resonantly enhanced at the L_{III} edge, since the non-resonant part is so large that it may mask the resonant behavior. On the other hand, the resonant enhancement of RXS intensities has clearly been observed on the superlattice spot $(00\frac{\ell}{2})$.

In this paper, we study the mechanism of the RXS spectra at the L_{III} edge in Phase II of DyB₂C₂. Since the $5d$ states are so extended in space that they are sensitive to lattice distortion caused by the buckling of sheets of B and C atoms. Then the question arises whether the direct influence of the lattice distortion on the $5d$ states is larger than the influence of the anisotropic $4f$ charge distribution associated with the quadrupole order through the $5d$ - $4f$ Coulomb interaction. Lovesey and Knight²¹ have discussed the mechanism from the symmetry viewpoint, and have pointed out that the RXS intensities on

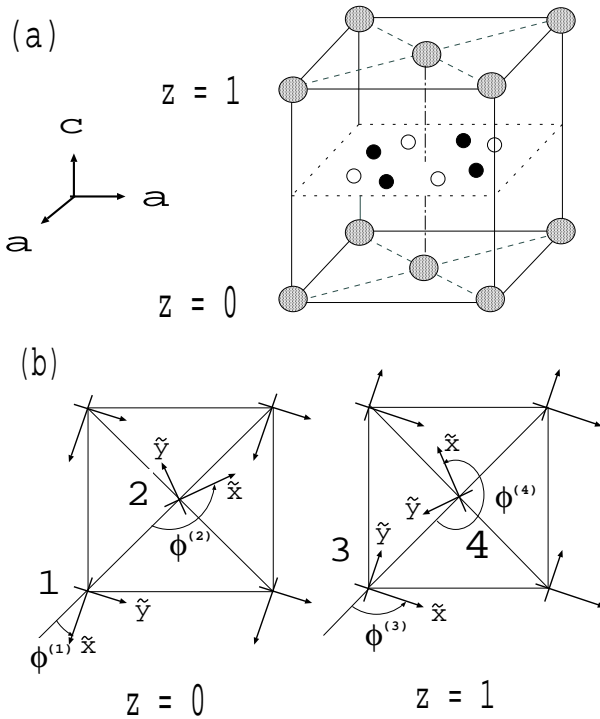


Fig. 1. (a) Sketch of the crystal structure of DyB_2C_2 ($P4/mbm$: $a = 5.341 \text{ \AA}$, $c = 3.547 \text{ \AA}$ at 30 K). Gray large circles are Dy atoms. Solid and open small circles are B and C atoms, respectively. (b) Local coordinate frames attached to each sublattice.

$(00\frac{\ell}{2})$ and $(h0\frac{\ell}{2})$ spots come from lowering the local symmetry probably due to lattice distortion. The argument based on symmetry alone is powerful in some respect, but does not shed light on this issue. In the transition-metal compounds, the corresponding question has already been answered by ab initio calculations as mentioned above. However, such ab initio calculations are difficult in rare-earth compounds. We resort to a model calculation by treating the $5d$ states as a band and the $4f$ states as localized states. The buckling of sheets of B and C atoms causes modulations of the $5d$ bands and of the $4f$ states. We analyze such effects of lattice distortion on the basis of the point charge model,²²⁾ which leads to four inequivalent Dy sites with principal axes of the crystal field shown in Fig. 1(b). These principal axes seem to correspond well to the direction of magnetic moments in the magnetic phase.¹⁹⁾ Of course, the point charge model is not good in quantitative viewpoint. Nonetheless, we construct an effective model that the $5d$ and $4f$ states are under the crystal field of the same form and with the same principal axes as the above analysis.

The crystal field modulates the $5d$ states. Although the actual effect may come from hybridizations to $2p$, $3s$ states of B and C, it can be included into a form of the crystal field. The crystal field also makes the quadrupole moment of the $4f$ states align along the principal axes, establishing a quadrupole order. A molecular field caused by the Dy-Dy interaction may also act on the $4f$ states in Phase II in addition to the crystal field. This interaction may be mediated by the RKKY interaction, but the explicit form has not been derived yet.

Note that the Ce-Ce interaction in CeB_6 has been extensively studied, describing well the phase diagram under the magnetic field.¹³⁻¹⁵⁾ But the molecular field may change little and even stabilize the quadrupole order. Therefore, we need not explicitly consider the molecular field by regarding the crystal field as including the effect. The charge anisotropy associated with the quadrupole order modulates the $5d$ states through the intra-atomic $5d$ - $4f$ Coulomb interaction.

We calculate the RXS intensity within the E_1 transition. We take account of the above two processes, direct and indirect ones, of modulating the $5d$ states. Both processes give rise to the RXS intensities on the $(00\frac{\ell}{2})$ and on the $(h0\frac{\ell}{2})$ spots. Both give similar photon-energy dependences and the same azimuthal-angle dependence in agreement with the experiment. However, the mechanism of direct modulation of the $5d$ band gives rise to the intensities much larger than the mechanism of indirect modulation through the $5d$ - $4f$ Coulomb interaction in a wide parameter range of the crystal field. This suggests that the RXS intensities are mainly controlled by the lattice distortion.

This paper is organized as follows. In § 2, we analyze the buckling of sheets of B and C atoms. In § 3, we briefly summarize the formulae used in the calculation of the RXS spectra. In § 4, we calculate the RXS spectra on two mechanisms. Section 5 is devoted to concluding remarks.

2. Lattice Distortion

For making clear the effect of lattice distortion on electronic states, we first calculate the electrostatic potential on the basis of a point charge model.²²⁾ Point charges q_{Dy} , q_{B} , and q_{C} are placed on Dy, B, and C sites, respectively. Figure 2 shows the positions of B and C atoms on the plane of $z = c/2$ and those of Dy atoms on the plane of $z = 0$. For the buckling of sheets of B and C atoms (up- and down-movements along the c axis) specified in Fig. 2, the electrostatic potential is evaluated within the second order of coordinates around Dy sites. As shown in Fig. 1(b), four inequivalent sites arises. For sites j ($= 1 \cdots 4$), the electrostatic potential is obtained as

$$V_{\text{crys}}(j) = A_2^0 Q_2^0 + A_2^2(j) Q_2^2 + A_{xy}(j) Q_{xy}, \quad (1)$$

with

$$Q_2^0 = \frac{1}{2}(3z^2 - r^2), \quad (2)$$

$$Q_2^2 = \frac{\sqrt{3}}{2}(x^2 - y^2), \quad (3)$$

$$Q_{xy} = \sqrt{3}xy, \quad (4)$$

where the coefficients are given by

$$A_2^0 = \frac{2q_{\text{D}}}{a^3} \left[1 - 2 \frac{|q_{\text{B}}|}{q_{\text{D}}} \left(\frac{a}{R_{\text{B}}} \right)^3 \left\{ 1 - 3 \left(\frac{c}{2R_{\text{B}}} \right)^2 \right\} - 2 \frac{|q_{\text{C}}|}{q_{\text{D}}} \left(\frac{a}{R_{\text{C}}} \right)^3 \left\{ 1 - 3 \left(\frac{c}{2R_{\text{C}}} \right)^2 \right\} \right]$$

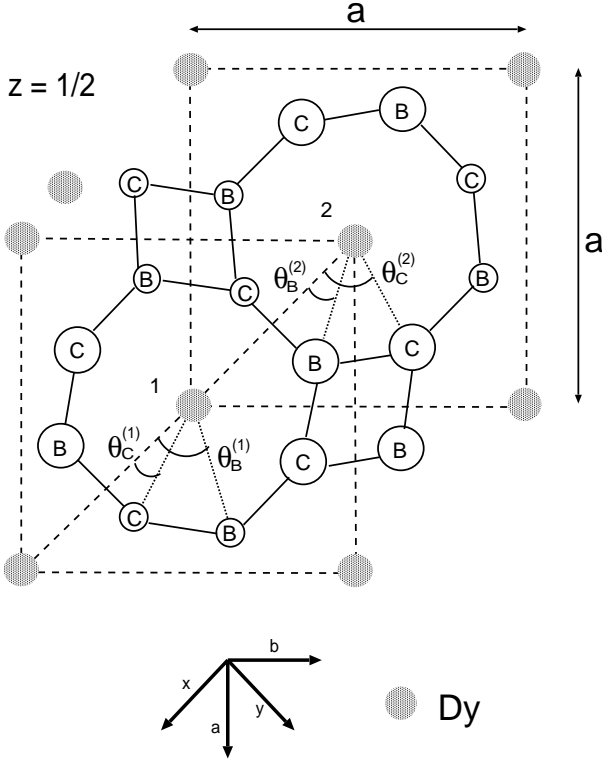


Fig. 2. Sketch of a B₂C₂ sheet ($z = c/2$). Open circles represent B and C atoms; big and small circles move to positive and negative directions along the z axis, respectively. The directions are reversed on the plane of $z = -c/2$. Hatched circles represent Dy atoms at the plane of $z = 0$.

$$= \frac{2q_D}{a^3} \left[1 + 1.40 \frac{|q_B|}{q_D} + 1.79 \frac{|q_C|}{q_D} \right], \quad (5)$$

$$A_2^2(j) = \Lambda_B \cos(2\theta_B^{(j)}) + \Lambda_C \cos(2\theta_C^{(j)}), \quad (6)$$

$$A_{xy}(j) = \Lambda_B \sin(2\theta_B^{(j)}) + \Lambda_C \sin(2\theta_C^{(j)}), \quad (7)$$

with

$$\begin{aligned} \Lambda_B &= -\frac{|q_B|}{a^3} \frac{60}{\sqrt{3}} \left(\frac{r_B}{a} \right)^2 \left(\frac{a}{R_B} \right)^5 \left(\frac{c}{2R_B} \right)^2 \frac{d_B}{\frac{c}{2}} \\ &= -22.3 \frac{|q_B|}{a^3} \frac{d_B}{\frac{c}{2}}, \end{aligned} \quad (8)$$

$$\begin{aligned} \Lambda_C &= -\frac{|q_C|}{a^3} \frac{60}{\sqrt{3}} \left(\frac{r_C}{a} \right)^2 \left(\frac{a}{R_C} \right)^5 \left(\frac{c}{2R_C} \right)^2 \frac{d_C}{\frac{c}{2}} \\ &= -24.0 \frac{|q_C|}{a^3} \frac{d_C}{\frac{c}{2}}. \end{aligned} \quad (9)$$

The first term in eq. (1) represents the crystal field without lattice distortion, while the second and third terms arise from the buckling. The R_B ($= 2.732\text{\AA}$) and R_C ($= 2.676\text{\AA}$) are distances from the origin to B and C sites, respectively. The d_B and d_C represent the absolute values of shifts along the c axis from the $z = \pm c/2$ planes, respectively. Angles $\theta_{B(C)}^{(j)}$ and $\theta_{B(C)}^{(j)}$ in eqs. (6) and (7) are given by

$$\theta_B^{(1)} = 65.6^\circ, \quad \theta_C^{(1)} = 19.1^\circ,$$

$$\theta_B^{(2)} = 180^\circ - 65.6^\circ, \quad \theta_C^{(2)} = 180^\circ - 19.1^\circ,$$

$$\theta_B^{(3)} = 90^\circ + \theta_B^{(1)}, \quad \theta_C^{(3)} = 90^\circ + \theta_C^{(1)},$$

$$\theta_B^{(4)} = 90^\circ + \theta_B^{(2)}, \quad \theta_C^{(4)} = 90^\circ + \theta_C^{(2)}. \quad (10)$$

Now we search for the local coordinate frames in which the third term in eq. (1) is eliminated. Rotating the original coordinate frame by angle ϕ_j around the c axis for each sublattice, we have the operators transformed as

$$Q_2^2 = \cos(2\phi_j) \tilde{Q}_2^2(j) - \sin(2\phi_j) \tilde{Q}_{xy}(j),$$

$$Q_{xy} = \sin(2\phi_j) \tilde{Q}_2^2(j) + \cos(2\phi_j) \tilde{Q}_{xy}(j), \quad (11)$$

where tilde operators $\tilde{Q}(j)$'s are represented with respect to the local coordinate frames. Q_2^0 is unchanged. Inserting eq. (11) into eq. (1), we have

$$V_{cryst}(j) = A_2^0 \tilde{Q}_2^0(j) + \tilde{A}_2^2(j) \tilde{Q}_2^2(j) + \tilde{A}_{xy}(j) \tilde{Q}_{xy}(j), \quad (12)$$

with

$$\tilde{A}_2^2(j) = \Lambda_B \cos[2(\theta_B^{(j)} - \phi_j)] + \Lambda_C \cos[2(\theta_C^{(j)} - \phi_j)], \quad (13)$$

$$\tilde{A}_{xy}(j) = \Lambda_B \sin[2(\theta_B^{(j)} - \phi_j)] + \Lambda_C \sin[2(\theta_C^{(j)} - \phi_j)]. \quad (14)$$

Condition $\tilde{A}_{xy}(j) = 0$ determines ϕ_j 's, which take values between $\theta_B^{(j)}$ and $\theta_C^{(j)}$. For example, assuming $q_B = q_C = -(3/4)e$, $q_{Dy} = 3e$ (e : proton charge), $d_B = 0.01\text{\AA}$, $d_C = 0.02\text{\AA}$, we have $\phi_1 = 31.8^\circ$, $\phi_2 = 180^\circ - \phi_1$, $\phi_3 = 90^\circ + \phi_1$, $\phi_4 = 90^\circ + \phi_2$. The principal axes thus estimated correspond well with the directions of the ordered magnetic moments in Phase III.¹⁹⁾

The equivalent operator method allows us to write the crystal field energy $H_{cryst}(j)$ at site j within the subspace of angular momentum J as

$$H_{cryst}(j) = D_J [3\tilde{J}_z^2(j) - J(J+1)] + E_J [\tilde{J}_x^2(j) - \tilde{J}_y^2(j)]. \quad (15)$$

(a) on the 5d bands

The 5d states are forming an energy band with width ~ 15 eV through a hybridization with s and p states of neighboring B and C atoms as well as 5d states of neighboring Dy atoms. We need the density of states (DOS) for calculating the RXS intensity. We assume a Lorentzian with full width of half maximum 5 eV for the DOS's projected onto symmetries xy , $x^2 - y^2$, yz , zx , and $3z^2 - r^2$. The center of each component of the DOS is separate to each other in accordance with the first term of eq. (15), although the first term need not be respected so much because of the large band effect. Explicitly they are assumed to be $(1/\pi)\Delta/((\epsilon - 2.5)^2 + \Delta^2)$ for xy , $x^2 - y^2$, $(1/\pi)\Delta/((\epsilon - 7)^2 + \Delta^2)$ for yz , zx , and $(1/\pi)\Delta/((\epsilon - 8.5)^2 + \Delta^2)$ for $3z^2 - r^2$, with energies in units of eV and $\Delta = 2.5$ eV. This arbitrary assumption for the DOS form may be justified by the fact that the RXS spectra is not sensitive to the assumption.

The second term of eq. (15), which arises from the buckling of sheets of B and C atoms, gives rise to a

small modification on the $5d$ band. Although the actual modulation of the $5d$ states may come through the hybridization to the s and p states of B and C atoms, such effects can be included into the second term. This term makes the local symmetry twofold.

(b) on the $4f$ states

Dy^{3+} ion is approximately in the $4f^9$ -configuration (${}^6\text{H}_{15/2}$). Equation (15) is now applied to the subspace of $J = 15/2$. Since the $4f$ states are much localized than the $5d$ states, the crystal field is much smaller here than that on the $5d$ states. The coefficient D_f of the first term is expected to be positive from the analysis of magnetic susceptibility.¹⁹⁾ This leads to the lowest energy states $|\pm \frac{1}{2}\rangle$ and the next energy states $|\pm \frac{3}{2}\rangle$, both of which form Kramers' doublets ($|M\rangle$ represents the state of $J_z = M$). The axial symmetry is kept instead of fourfold symmetry without the lattice distortion. Terms of $O_4^4 \equiv \frac{1}{2}(J_+^4 + J_-^4)$, which admixes the states $|M\rangle$ with $|M \pm 4\rangle$, come from the higher order expansion to make the local symmetry fourfold. The detailed study along this line, however, is beyond the scope of the present study.

In any event, the second term makes the local symmetry twofold. The lowest energy state is admixed by $|M\rangle$ with $|M| > 1/2$. The quadrupole moment is ordered; $\langle \tilde{O}_{x^2-y^2} \rangle (\equiv \frac{\sqrt{3}}{2} \langle \tilde{J}_x^2 - \tilde{J}_y^2 \rangle)$ takes a finite value with $\langle \tilde{O}_{xy} \rangle (\equiv \frac{\sqrt{3}}{2} \langle \tilde{J}_x \tilde{J}_y + \tilde{J}_y \tilde{J}_x \rangle) = 0$ in the local coordinate frame for each sublattice ($\langle \dots \rangle$ means the average over the lowest Kramers doublet). With increasing values of $|E_f|/D_f$, the average quadrupole moment increases, as shown in Fig. 6(b). It becomes largest, $\langle \tilde{O}_{x^2-y^2} \rangle = 46.1$ at $D_f = 0.1$.

3. Cross Section of Resonant X-Ray Scattering

We briefly summarize here the formulae used in the calculation of the RXS spectra in the next section. The conventional RXS geometry is shown in Fig. 3; photon with frequency ω , momentum \mathbf{k}_i and polarization μ ($= \sigma$ or π) is scattered into the state with momentum \mathbf{k}_f and polarization μ' ($= \sigma'$ or π'). The scattering vector is defined as $\mathbf{G} \equiv \mathbf{k}_f - \mathbf{k}_i$. Near the Dy L_{III} absorption edge, a $2p$ core electron is virtually excited to $5d$ states in the E_1 process. Subsequently it recombines with the core hole. Since the $2p$ states are well localized around Dy sites, it is a good approximation to describe the scattering tensor as a sum of contributions from each site of the core hole. Therefore, the cross section in the E_1 process is given by

$$I_{\mu \rightarrow \mu'}(\mathbf{G}, \omega) \propto \left| \sum_{\alpha\alpha'} P_{\alpha}^{\mu\mu'} M_{\alpha\alpha'}(\mathbf{G}, \omega) P_{\alpha'}^{\mu} \right|^2, \quad (16)$$

where

$$M_{\alpha\alpha'}(\mathbf{G}, \omega) = \frac{1}{\sqrt{N}} \sum_j M_{\alpha\alpha'}(j, \omega) \exp(-i\mathbf{G} \cdot \mathbf{r}_j), \quad (17)$$

with

$$M_{\alpha\alpha'}(j, \omega) = \sum_{\Lambda} \frac{\langle \psi_n | x_{\alpha}(j) | \Lambda \rangle \langle \Lambda | x_{\alpha'}(j) | \psi_j \rangle}{\hbar\omega - (E_{\Lambda} - E_j) + i\Gamma}, \quad (18)$$

Table I. Geometrical factors

α	$(P^{\sigma})_{\alpha}$	$(P^{\sigma'})_{\alpha}$	$(P^{\pi'})_{\alpha}$
1	$\cos \beta \cos \psi$	$\cos \beta \cos \psi$	$-\sin \theta \cos \beta \sin \psi + \cos \theta \sin \beta$
2	$-\sin \psi$	$-\sin \psi$	$-\sin \theta \cos \psi + \cos \theta \sin \beta$
3	$-\sin \beta \cos \psi$	$-\sin \beta \cos \psi$	$\cos \theta \cos \beta$

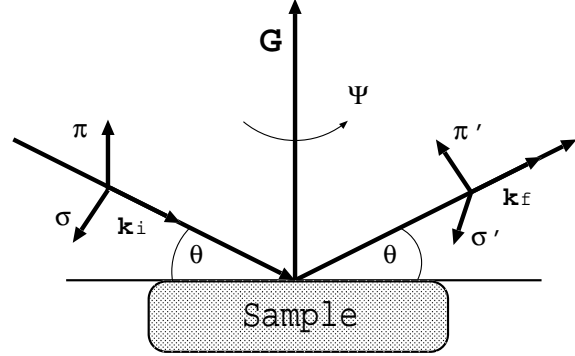


Fig. 3. Scattering geometry. Incident photon with wave vector \mathbf{k}_i and polarization σ or π is scattered into the state with wave vector \mathbf{k}_f and polarization σ' or π' at Bragg angle θ . The sample crystal is rotated by azimuthal angle ψ around the scattering vector $\mathbf{G} = \mathbf{k}_f - \mathbf{k}_i$.

where N is the number of Dy sites. Note that the cross section is an order of N . The P^{μ} and $P^{\mu'}$ are geometrical factors for the incident and scattered photons, respectively. Their explicit forms are given in Table I. The $|\psi_j\rangle$ represents the initial state with energy E_j . The intermediate state $|\Lambda\rangle$ consists of an excited electron on $5d$ states and a hole on $2p$ states with energy E_{Λ} . The Γ is the life-time broadening width of the core hole. The dipole operators $x_{\alpha}(j)$'s are defined as $x_1(j) = x$, $x_2(j) = y$, and $x_3(j) = z$ in the coordinate frame fixed to the crystal axes with the origin located at the center of site j . The scattering amplitude $M_{\alpha\alpha'}(\mathbf{G}, \omega)$ contains the square of the dipole matrix element $A_{dp} = \langle 5d|r|2p \rangle = \int_0^{\infty} R_{5d}(r)rR_{2p}(r)r^2 dr$ with $R_{5d}(r)$ and $R_{2p}(r)$ being the radial wavefunctions for the $5d$ and $2p$ states. For Dy^{3+} atom, it is estimated as 2.97×10^{-11} cm in the $4f^9$ configuration within the HF approximation.²³⁾

4. Calculation of RXS spectra

In the E_1 transition, an electron is excited from $2p$ states to $5d$ states at a Dy site. A $2p$ core hole is left behind, and its state is split into the states of $j_p = 3/2$ and $j_p = 1/2$ (j_p is the total angular momentum) due to the strong spin-orbit interaction. We consider only the $j_p = 3/2$ states (L_{III} edge). We describe the photoexcited $5d$ electron in the band by introducing a local Green's function,

$$G_{m^d}^{5d}(\hbar\omega) = \int_{\epsilon_F}^{\infty} \frac{\rho_{m^d}^{5d}(\epsilon)}{\hbar\omega - \epsilon + i\delta} d\epsilon, \quad (19)$$

where $\rho_{m^d}^{5d}(\epsilon)$ is the m^d component of the d DOS defined in §2. The Fermi energy ϵ_F is set to be zero so that the

Table II. Slater integrals and the spin-orbit interaction for Dy³⁺ atoms in the Hartree-Fock approximation (in units of eV).

$F^k(4f, 4f)$	$F^k(2p, 5d)$	$F^k(2p, 4f)$	$F^k(4f, 5d)$
F^0 32.19	F^0 16.13	F^0 44.62	F^0 14.70
F^2 15.31	F^2 0.489	F^2 1.982	F^2 3.614
F^4 9.607			F^4 1.741
F^6 6.911			
	$G^k(2p, 5d)$	$G^k(2p, 4f)$	$G^k(4f, 5d)$
	G^1 0.414	G^2 0.207	G^1 1.615
	G^3 0.245	G^4 0.133	G^3 1.321
			G^5 1.009
$\zeta_{4f} = 0.273$		$\zeta_{5d} = 0.181$	

*In the RXS calculation, the above values of the anisotropic terms are reduced by multiplying a factor 0.8, while the values for $F^{(0)}(nl, n'l')$ are replaced by much smaller values, $F^{(0)}(4f, 5d) = 3.0$, $F^{(0)}(4f, 4f) = 7.0$, $F^{(0)}(2p, 5d) = 4.0$, $F^{(0)}(2p, 4f) = 12.0$.

5d band is almost empty.

Finite RXS intensities on superlattice spots arise from modulating the 5d states with wave vectors of superlattice spots. There are two origins to giving rise to such modulation. One is a direct influence from the buckling of sheets of B and C atoms, which is represented by the second term of eq. (15). Another is the charge anisotropy of the 4f states in the quadrupole ordering phase. We discuss both origins separately. In the actual calculation, we specify the local coordinate frames with $\phi_1 = 28^\circ$, $\phi_2 = 180^\circ - 28^\circ$, $\phi_3 = 90^\circ + 28^\circ$, $\phi_4 = 90^\circ + 152^\circ$ for four sublattices in accordance with the experiment.¹⁹⁾

4.1 Direct influence of lattice distortion

Let the E_1 transition take place at a particular site (called as ‘‘origin’’). The excited 5d electron is attracted by the core hole potential at the origin. What is more important is that the 5d electron is under the influence of the second term of eq. (15). Taking account of the multiple scattering from these terms at the origin, we evaluate the resolvent $1/(\hbar\omega - H_{\text{int}})$ with respect to the intermediate-state Hamiltonian H_{int} :

$$\begin{aligned} & \left(\frac{1}{\hbar\omega - H_{\text{int}} + i\Gamma} \right)_{m^d s^d \lambda; m'^d s'^d \lambda'} \\ &= [G_{m^d}^{5d} (\hbar\omega + i\Gamma - \epsilon_\lambda)^{-1} \delta_{\lambda\lambda'} \delta_{m^d m'^d} \delta_{s^d s'^d} \\ & \quad - V_{m^d s^d \lambda; m'^d s'^d \lambda'}]^{-1}, \end{aligned} \quad (20)$$

where m^d and s^d specify the orbital and spin of the d electron, respectively. The ϵ_λ represents the energy of the core hole with λ in the $j_p = 3/2$ subspace. The scattering potential $V_{m^d s^d \lambda; m'^d s'^d \lambda'}$ includes the second term of eq. (15) and the Coulomb interaction between the 5d electron and the 2p hole. The latter quantity is expressed in terms of the Slater integrals, which are evaluated within the HF approximation in a Dy³⁺ atom (see Table II).²⁴⁾ The core hole life-time width is set to be $\Gamma = 2.5$ eV. Equation (20) is numerically evaluated.

Before calculating the RXS spectra, we touch on the absorption coefficient. We calculate the absorption coefficient $A(\omega)$ in the E_1 process from the resolvent by

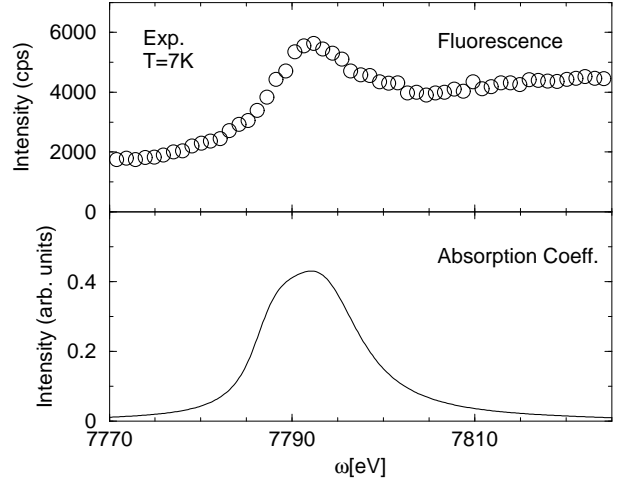


Fig. 4. Absorption coefficient $A(\omega)$ (lower panel) in comparison with the L_{III} -edge fluorescence spectra (upper panel).¹⁷⁾

using the relation,

$$\begin{aligned} A(\omega) &\propto \sum_j \sum_\alpha \langle \psi_j | x^\alpha(j) | m^d s^d \lambda \rangle \\ &\times \left(-\frac{1}{\pi} \right) \text{Im} \left(\frac{1}{\hbar\omega - H_{\text{int}} + i\delta} \right)_{m^d s^d \lambda; m'^d s'^d \lambda'} \\ &\times \langle m'^d s'^d \lambda' | x^\alpha(j) | \psi_j \rangle. \end{aligned} \quad (21)$$

Here $\text{Im}X$ indicates the imaginary part of the quantity X . Figure 4 shows the calculated $A(\omega)$ in comparison with the fluorescence experiment.¹⁷⁾ We adjust the core hole energy such that the calculated peak coincides with the experimental one. The calculated curve reproduces the experimental one. Since the spectra is proportional to the d DOS when the 5d-2p Coulomb interaction is neglected, the assumed DOS seems reasonable. The intensity seen in the high energy region of the experiment may come from the d symmetric states mixing with 3s, 3p states of B and C atoms, which is outside our interest.

Now we discuss the RXS spectra. The resolvent above calculated is used to calculate the scattering amplitude at the origin with the help of the relation,

$$\begin{aligned} & \sum_\Lambda \frac{|\Lambda\rangle\langle\Lambda|}{\hbar\omega - (E_\Lambda - E_j) + i\Gamma} \\ &= \sum_{m^d s^d \lambda} \sum_{m'^d s'^d \lambda'} |m^d s^d \lambda\rangle \\ &\times \left(\frac{1}{\hbar\omega - H_{\text{int}} + i\Gamma} \right)_{m^d s^d \lambda; m'^d s'^d \lambda'} \langle m'^d s'^d \lambda' |. \end{aligned} \quad (22)$$

This expression is independent of the quadrupole ordering 4f states. It is inserted into eq. (18) to calculate an RXS amplitude. The extension to general site j is straightforward. In the coordinate frame fixed to crystal (not in the local coordinate frames), their forms are

given by

$$\begin{aligned}\hat{M}(1, \omega) &= \begin{pmatrix} \xi(\omega) & \eta(\omega) & 0 \\ \eta(\omega) & \zeta(\omega) & 0 \\ 0 & 0 & \gamma(\omega) \end{pmatrix}, \\ \hat{M}(2, \omega) &= \begin{pmatrix} \zeta(\omega) & \eta(\omega) & 0 \\ \eta(\omega) & \xi(\omega) & 0 \\ 0 & 0 & \gamma(\omega) \end{pmatrix}, \\ \hat{M}(3, \omega) &= \begin{pmatrix} \zeta(\omega) & -\delta(\omega) & 0 \\ -\delta(\omega) & \xi(\omega) & 0 \\ 0 & 0 & \gamma(\omega) \end{pmatrix}, \\ \hat{M}(4, \omega) &= \begin{pmatrix} \xi(\omega) & -\delta(\omega) & 0 \\ -\delta(\omega) & \zeta(\omega) & 0 \\ 0 & 0 & \gamma(\omega) \end{pmatrix}.\end{aligned}\quad (23)$$

(a) $\mathbf{G} = (00\frac{\ell}{2})$ with ℓ odd integers.

Owing to the factor $\exp(-i\mathbf{G} \cdot \mathbf{r}_j)$ in eq. (17), the total amplitude is given by a combination of $\hat{M}(1, \omega) + \hat{M}(2, \omega) - \hat{M}(3, \omega) - \hat{M}(4, \omega)$. Thus, we have the final form,

$$\frac{\hat{M}(\mathbf{G}, \omega)}{\sqrt{N}} = \begin{pmatrix} 0 & \eta(\omega) & 0 \\ \eta(\omega) & 0 & 0 \\ 0 & 0 & 0 \end{pmatrix}.\quad (24)$$

The geometrical factors are given by setting $\beta = 0$ in Table I, which are combined to eq. (24) to calculate the scattering intensity. We have the RXS intensity as a function of azimuthal angle ψ as

$$\begin{aligned}I_{\sigma \rightarrow \sigma'}(\mathbf{G}, \omega) &\propto |\eta(\omega)|^2 \sin^2 2\psi, \\ I_{\sigma \rightarrow \pi'}(\mathbf{G}, \omega) &\propto |\eta(\omega)|^2 \sin^2 \theta \cos^2 2\psi,\end{aligned}\quad (25)$$

with θ the Bragg angle. Here ψ is defined such that $\psi = 0$ corresponds to the scattering plane containing the b axis.

Figure 5 shows the calculated RXS spectra as a function of photon energy in comparison with the experiment ($\psi = -45^\circ$).¹⁷ The crystal field parameter is set to be $E_d = -0.1$ eV in eq. (15). As shown in the middle panel, the calculated spectra show a single-peak in agreement with the experiment. (Only the $\sigma \rightarrow \sigma'$ channel gives finite intensity for $\psi = -45^\circ$.) The photon energy dependence in the $\sigma \rightarrow \pi'$ channel is found to be the same as in the $\sigma \rightarrow \sigma'$ channel in the calculation. On the other hand, an extra peak has been observed in the $\sigma \rightarrow \pi'$ channel at $\hbar\omega = 7782$ eV (pre-edge peak) for $\psi = 0$.¹⁷ This peak may come from the electric quadrupole (E_2) transition.

Figure 6(a) plots the peak intensity as a function of $|E_d|$ (at $\psi = -45^\circ$ in the $\sigma \rightarrow \sigma'$ channel). The intensity of the “main” peak increases with increasing values of $|E_d|$. It is nearly proportional to $|E_d|^2$.

Figure 7 shows the azimuthal angle dependence of the main peak intensity for $\mathbf{G} = (00\frac{\ell}{2})$, in good agreement with the experiment. The same dependence as eq. (25) has been proposed on the basis of the symmetry of the scattering tensor.¹⁸ Note that the intensity ratio between the $\sigma \rightarrow \sigma'$ channel and the $\sigma \rightarrow \pi'$ channel is determined by a geometrical factor; the oscillation am-

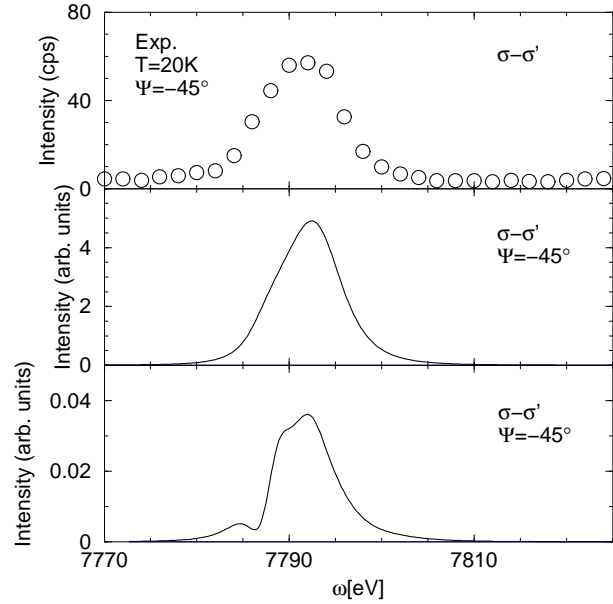


Fig. 5. RXS spectra for $\mathbf{G} = (00\frac{5}{2})$ at $\psi = -45^\circ$ in the $\sigma \rightarrow \sigma'$ channel, as a function of photon energy. Top: experimental spectra at $T = 20$ K (Phase II).¹⁷ Middle: Calculated spectra by taking account of the direct influence of lattice distortion with $E_d = -0.1$ eV. Bottom: Calculated spectra by taking account of the influence of quadrupole ordering $4f$ states with $E_f/D_f = -0.2$.

plitude of intensity in the $\sigma \rightarrow \pi'$ channel is the factor $\sin^2 \theta = 0.312$ smaller than that in the $\sigma \rightarrow \sigma'$ channel.

(b) $\mathbf{G} = (h0\frac{\ell}{2})$ with h and ℓ odd integers.

The total amplitude is given by a combination of $\hat{M}(1, \omega) - \hat{M}(2, \omega) - \hat{M}(3, \omega) + \hat{M}(4, \omega)$. Thus, we have the final form,

$$\frac{\hat{M}(\mathbf{G}, \omega)}{\sqrt{N}} = \begin{pmatrix} \frac{1}{2}(\xi(\omega) - \zeta(\omega)) & 0 & 0 \\ 0 & \frac{1}{2}(\zeta(\omega) - \xi(\omega)) & 0 \\ 0 & 0 & 0 \end{pmatrix}.\quad (26)$$

Combining the geometrical factor in Table I to eq. (26), we obtain the scattering intensity. The spectral shape as a function of photon energy is found almost the same as that for the $(00\frac{\ell}{2})$ spot, so that we omit the corresponding figure. The azimuthal angle dependence is given by

$$\begin{aligned}I_{\sigma \rightarrow \sigma'}(\mathbf{G}, \omega) &\propto \frac{1}{4}|\xi(\omega) - \zeta(\omega)|^2 (\cos^2 \beta \cos^2 \psi - \sin^2 \psi)^2, \\ I_{\sigma \rightarrow \pi'}(\mathbf{G}, \omega) &\propto \frac{1}{4}|\xi(\omega) - \zeta(\omega)|^2 \\ &\quad \times [\cos \theta \sin \beta (\cos \beta \cos \psi + \sin \psi) \\ &\quad - \sin \theta (1 + \cos^2 \beta) \sin \psi \cos \psi]^2,\end{aligned}\quad (27)$$

where β is determined from $\tan \beta = (2hc)/(\ell a)$. Figure 8 shows the azimuthal dependence of the peak intensity for the $(30\frac{3}{2})$ spot. A large non-resonant intensity has been observed in the $\sigma \rightarrow \sigma'$ channel, and the resonant behavior is not clear in the experiment.^{16, 17} The non-resonant intensity may come from the Thomson scattering due to the lattice distortion. We hope that the resonant behavior discussed here is observed in the $\sigma \rightarrow \pi'$ channel, since the non-resonant intensity is expected to disappear

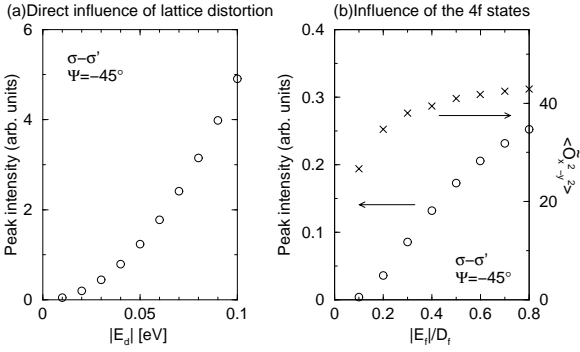


Fig. 6. (a) Main peak intensity as a function of the crystal field parameter $|E_d|$ on the $5d$ states, which is calculated by taking account of the direct influence of lattice distortion. (b) Main peak intensity as a function of the crystal field parameter $|E_f|/D_f$ on the $4f$ states, which is calculated by taking account of the influence of quadrupole ordering $4f$ states (open circles). Crosses represent the quadrupole moments $\langle \hat{O}_{x^2-y^2} \rangle$ in the local coordinate frame for each sublattice.

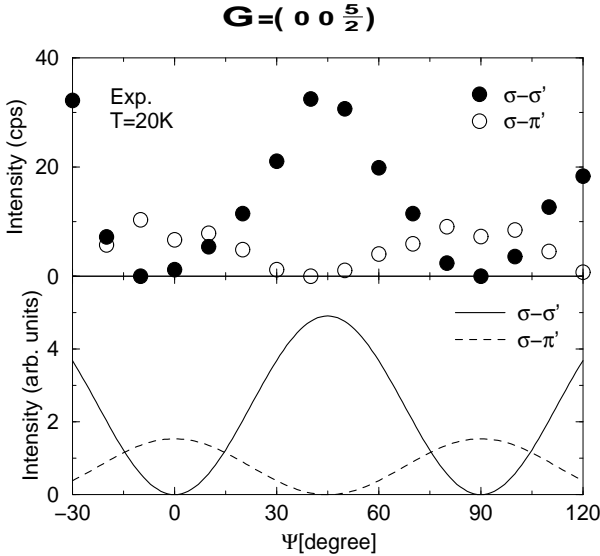


Fig. 7. Azimuthal angle dependence of the RXS intensity of the main peak on $\mathbf{G} = (00\frac{5}{2})$, in comparison with the experiment at $T = 20$ K.¹⁷⁾

in this channel.

4.2 Influence of quadrupole ordering $4f$ states

The initial state is evaluated in § 2, where the $4f$ quadrupole moment is ordered. The intermediate state is evaluated by the following steps. Let the E_1 transition take place at the origin. The complex of $4f$ electrons and the $2p$ hole is assigned as the eigenstate $|\nu\rangle$ with energy E_ν , which is calculated by diagonalizing the matrix of the intra-atomic Coulomb interaction. To keep the matrix size manageable, the space of $4f$ states is restricted within the space of $J = 15/2$. This restriction causes only minor errors in the RXS spectra, since the RXS amplitude contains the overlap between the $4f$ states in the intermediate state and that in the initial state, which becomes very small for the $4f$ states outside the $J = 15/2$ subspace. Since the photoexcited $5d$ electron interacts

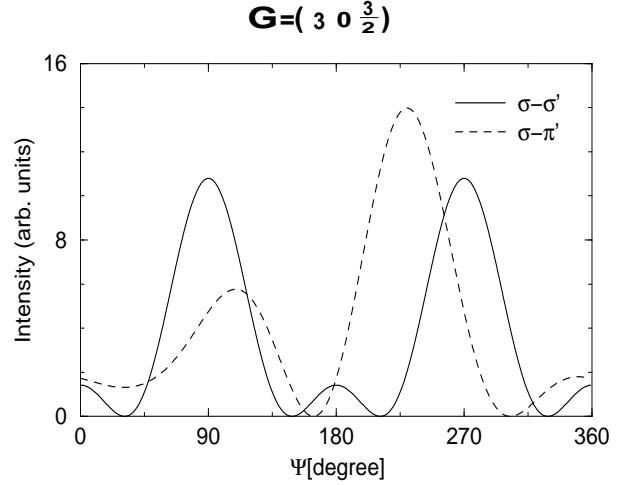


Fig. 8. Azimuthal angle dependence of the RXS intensity of the main peak on $\mathbf{G} = (30\frac{3}{2})$.

with the $2p$ hole and with $4f$ electrons, the complex of $4f$ electrons and the $2p$ hole serves as a scatterer to the $5d$ electron. Thus we have the resolvent at the origin,

$$\begin{aligned} & \left(\frac{1}{\hbar\omega - H_{\text{int}} + i\Gamma} \right)_{m^d s^d \nu; m'^d s'^d \nu'} \\ &= [G_{m^d}^{5d} (\hbar\omega + i\Gamma - E_\nu)^{-1} \delta_{\nu\nu'} \delta_{m^d m'^d} \delta_{s^d s'^d} \\ & \quad - U_{m^d s^d \nu; m'^d s'^d \nu'}]^{-1}, \end{aligned} \quad (28)$$

where m^d and s^d specify $5d$ states. The potential $U_{m^d s^d \nu; m'^d s'^d \nu'}$ includes the $5d$ - $4f$ Coulomb interaction as well as the $5d$ - $2p$ Coulomb interaction. They are expressed in terms of the Slater integrals, which are given in Table II.^{23,24)} Since the $5d$ - $4f$ Coulomb interaction is implicitly included in the $5d$ -band energy, we eliminate the average of the $5d$ - $4f$ interaction from the potential U . The energies of the $4f$ states coming from the crystal field much smaller than other energies in the intermediate state, and thus can be neglected. We do not include the crystal field on the $5d$ states due to the lattice distortion (the second term of eq. (15)). Within the present approximation, the right hand side of eq. (28) becomes a matrix with dimensions 640×640 ($640 = 10 \times 64$), which are numerically inverted.

The resolvent thus obtained is the same on four sublattices. The scattering amplitudes become different on different sublattices after the transition matrix elements from the initial state are taken into account. The scattering amplitude is found to take the same forms as eqs. (23). Therefore, the azimuthal-angle dependence is the same as eqs. (25) and (27). As regards the photon-energy dependence, the bottom panel in Fig. 5 shows the RXS spectra at $\psi = -45^\circ$ in the $\sigma \rightarrow \sigma'$ channel for $\mathbf{G} = (00\frac{5}{2})$. We put $E_f/D_f = -0.2$. The spectral shape is not so different from the curve given in the preceding subsection, although a small hump appears at the low energy side. Difference is the magnitude of the intensity. Figure 6(b) shows the main-peak intensity as a function of $|E_f|/D_f$. It increases with increas-

ing values of $|E_f|/D_f$. In the same figure, we have also plotted the sublattice quadrupole moment as a function of $|E_f|/D_f$. It also increases with increasing values of $|E_f|/D_f$. This coincidence is plausible, since the charge anisotropy in the $4f$ states increases with increasing the ordered quadrupole moment. However, its magnitude remains much smaller than those given by the direct influence of lattice distortion in a wide parameter range of crystal field by comparison with the curve in Fig. 6(a).

5. Concluding Remarks

We have studied the mechanism of RXS at the L_{III} edge in the quadrupole ordering phase of DyB_2C_2 . Having analyzed the effect of the bucking of sheets of B and C atoms on the $5d$ and $4f$ states, we have constructed an effective model that the crystal field is acting on the $5d$ and $4f$ states with the principal axes different for different sublattices. We have calculated the RXS spectra in the E_1 process by treating the $5d$ states as a band and the $4f$ states as localized states. We have considered two mechanisms separately that the lattice distortion directly modulates the $5d$ band and that the charge anisotropy of the quadrupole ordering $4f$ states modulate the $5d$ band through the $5d$ - $4f$ intra-atomic Coulomb interaction. We have found that both mechanisms give rise to the RXS intensities on $(00\frac{L}{2})$ and $(h0\frac{L}{2})$ spots with similar photon-energy dependences and the same azimuthal angle dependence. Both explain well the experimental RXS spectra. However, it is shown that the former mechanism gives rise to the intensity much larger than the latter one for a wide parameter range of crystal field. This suggests that the main-peak of the RXS spectra is not a direct reflection of the quadrupole order but mainly controlled by the lattice distortion. To confirm this observation more quantitatively, band structure calculations may be useful since the $5d$ states are considerably extended in space. This study is left in the future.

As regards the pre-edge peak, we have estimated its intensity within the E_2 transition. In that estimate, we have used the same initial state as discussed above and have taken account of the full multiplets of the f^{10} -configuration for the intermediate state. The transition matrix element has been evaluated by the atomic Hartree-Fock wave function.²³⁾ The pre-edge peak intensity thus evaluated is found to be more than three-order of magnitude smaller than the main-peak intensity evaluated by the mechanism of the charge anisotropy of the quadrupole ordering $4f$ states. This is inconsistent with the experiments, where the pre-edge peak intensity is the same order of magnitude to the main peak intensity. Clarifying this point is also left in the future.

Acknowledgments

We would like to thank S. W. Lovesey, Y. Tanaka, and T. Inami for valuable discussions. This work was partially supported by a Grant-in-Aid for Scientific Research from the Ministry of Education, Science, Sports and Culture.

- 1) Y. Murakami, H. Kawata, M. Tanaka, T. Arima, Y. Moritomo and Y. Tokura: Phys. Rev. Lett. **80** (1998) 1932.
- 2) Y. Murakami, J. P. Hill, D. Gibbs, M. Blume, I. Koyama, M. Tanaka, H. Kawata, T. Arima, Y. Tokura, K. Hirota and Y. Endoh: Phys. Rev. Lett. **81** (1998) 582.
- 3) M. von Zimmermann, J.P. Hill, D. Gibbs, M. Blume, D. Casa, B. Keimer, Y. Murakami, Y. Tomioka and Y. Tokura: Phys. Rev. Lett. **83** (1999) 4872.
- 4) M. Noguchi, A. Nakazawa, T. Arima, Y. Wakabayashi, H. Nakao and Y. Murakami: Phys. Rev. B **62** (2000) R9271.
- 5) S. Ishihara and S. Maekawa: Phys. Rev. Lett. **80** (1998) 3799.
- 6) I. S. Elfimov, V. I. Anisimov and G. Sawatzky: Phys. Rev. Lett. **82** (1999) 4264.
- 7) M. Benfatto, Y. Joly and C. R. Natoli: Phys. Rev. Lett. **83** (1999) 636.
- 8) M. Takahashi, J. Igarashi and P. Fulde: J. Phys. Soc. Jpn. **68** (1999) 2530.
- 9) M. Takahashi, J. Igarashi and P. Fulde: J. Phys. Soc. Jpn. **69** (2000) 1614.
- 10) H. Nakao, K. Magishi, Y. Wakabayashi, Y. Murakami, K. Koyama, K. Hirota, Y. Endoh and S. Kunii: J. Phys. Soc. Jpn. **70** (2001) 1857.
- 11) T. Nagao and J. Igarashi: J. Phys. Soc. Jpn. **70** (2001) 2892.
- 12) J. Igarashi and T. Nagao: J. Phys. Soc. Jpn. **71** (2002) 1771.
- 13) R. Shiina, H. Shiba and P. Thalmeier: J. Phys. Soc. Jpn. **66** (1997) 1741.
- 14) O. Sakai, R. Shiina, H. Shiba and P. Thalmeier: J. Phys. Soc. Jpn. **66** (1997) 3005.
- 15) H. Shiba, O. Sakai and R. Shiina: J. Phys. Soc. Jpn. **68** (1999) 1988.
- 16) Y. Tanaka, T. Inami, T. Nakamura, H. Yamauchi, H. Onodera, K. Ohoyama and Y. Yamaguchi: J. Phys. Condens. Matter **11** (1999) L505.
- 17) K. Hirota, N. Oumi, T. Matsumura, H. Nakao, Y. Wakabayashi, Y. Murakami and Y. Endoh: Phys. Rev. Lett. **84** (2000) 2706.
- 18) T. Matsumura, N. Oumi, K. Hirota, H. Nakao, Y. Murakami, Y. Wakabayashi, T. Arima, S. Ishihara and Y. Endoh: Phys. Rev. B **65** (2002) 094420.
- 19) H. Yamauchi, H. Onodera, K. Ohoyama, T. Onimaru, M. Kosaka, M. Ohashi and Y. Yamaguchi: J. Phys. Soc. Jpn. **68** (1999) 2057.
- 20) H. Adachi, H. Kawata, M. Mizumaki, T. Akao, M. Sato, N. Ikeda, Y. Tanaka and H. Miwa: Phys. Rev. Lett. **89** (2002) 206401.
- 21) S. W. Lovesey and K. S. Knight: Phys. Rev. B **64** (2001) 094401.
- 22) M. T. Hutchings: Solid State Physics, **16** (1964) 227.
- 23) R. Cowan: The Theory of Atomic Structure and Spectra (University of California Press, Berkeley, 1981).
- 24) The anisotropic terms of the Coulomb interaction are slightly reduced in solids; we use the atomic values in Table II by reducing them with multiplying a factor 0.8. On the other hand, the values of $F^0(nl, n'l')$ are considerably screened in solids, so that they are replaced by much smaller values.